Electronic structure and thermoelectric properties of Sb-based semiconducting half-Heusler compounds

Mal-Soon Lee, Ferdinand P. Poudeu, and S. D. Mahanti

Phys. Rev. B **83**, 085204 — Published 17 February 2011

DOI: 10.1103/PhysRevB.83.085204

Electronic structure and thermoelectric properties of Sb-based semiconducting half-Heusler compounds

Mal-Soon Lee[1,2], Ferdinand P. Poudeu[2] and S. D. Mahanti[1]
[1] *Department of Physics and Astronomy, Michigan State University, East Lansing, MI 48824*
[2] *2Advanced Materials Research Institute and Department of Chemistry, University of New Orleans, New Orleans, LA 70148*

Electronic structure and transport properties of four Sb-based semiconducting half-Heusler compounds, *MA*Sb, where *M*=Hf or Zr and *A*=Co or Ir are studied using density-functional-theory and Boltzmann transport equation in constant relaxation time (τ) approximation. We find that substituting Hf with Zr does not change the band structures of these systems significantly. In contrast, replacing Co by Ir leads to drastic changes in their electronic structures. The valence band maximum occurs at the *L* point in the Co-compounds while it is at the Γ point in the Ir-compounds. The position and hybridization of a *s*-like conduction band vis-à-vis the hybridized *d*-bands of Co(Ir) determines the nature of the conduction bands near the band gap region. In addition, there is a direct band gap at the Γ point in HfIrSb, whereas in the other three compounds, the band gap is indirect, either between Γ and *X*, or between *L* and *X* points. The Co compounds usually give large thermopowers, both for *p*- and *n*-dopings. However ZrIrSb, due to its interesting conduction band structure, gives the best *n*-type thermopower at high temperatures. We discuss in detail how the subtle changes in the electronic structure near the band gap affects *S*, σ/τ, and the power factor.

PACS numbers: 71.15.Mb, 71.20.-b, 72.20.Pa, 84.60.Rb

I. INTRODUCTION

Thermoelectric (TE) materials are used for power generation and refrigeration. The efficiency of thermoelectric energy conversion depends on the transport coefficients of a TE material through the dimensionless figure of merit $ZT = \sigma S^2 T/\kappa$, where σ is the electrical conductivity, S is the thermopower (or Seebeck coefficient), T is temperature, and κ is the thermal conductivity. The thermal conductivity is given by the sum of contributions from the electronic carriers (κ_{el}) and the lattice (κ_l). The efficiency approaches the Carnot limit when $ZT \to \infty$. To increase ZT, S and σ have to be increased and κ has to be decreased. However, increasing σ by increasing the carrier concentration usually decreases the magnitude of S and increases κ_{el}. It is therefore a challenging task to increase ZT. Doped narrow band gap semiconductors are good thermoelectrics, because in these systems due to low carrier concentration κ_l usually dominates κ_{el}. One can therefore hope to manipulate the numerator of ZT, σS^2, known as the power factor (PF), and the denominator κ of the ZT independently. The former can be achieved by engineering the electronic structure and the latter by introducing phonon scatterers without affecting the electron transport, known as the electron crystal phonon glass concept.[1,2]

Half-Heuslers (HH) are ternary compounds with MgAgAs structure.[3] This structure consists of four interpenetrating face-center-cubic (FCC) sub-lattices where three of them contain one of the three elements each and the fourth sublattice is vacant. When the valence electron count (VEC) is 18 per unit cell, the HH compounds become semiconductors[4–9] and depending on their band gaps some of them show good thermoelectric properties such as large S and reasonably high σ at high temperatures,[10–12] and are therefore promising TE materials for power generation.

It is observed experimentally that *M*NiSn-based HH systems, where *M* = Ti, Hf, Zr, exhibit excellent *n*-type properties with large power factors (PF) resulting in a ZT of 0.8 at 1000 K.[13] For the *p*-type on the other hand, *M*CoSb compounds, where *M* = Ti, Hf, Zr, appear to be promising at high temperatures and they have been extensively studied experimentally.[14–21] At low temperatures these Co-based systems show some unusual behavior. Xia *et al.* observed that at room temperature (T = 300 K), TiCoSb shows a large negative (*n*-type) thermopower (S = -265 μV/K) with semiconductor-like resistivity, while ZrCoSb and HfCoSb show semimetallic resistivity and reduced thermopower of S = -10 μV/K.[14] They also observed that an appropriate substitution of Sn into these compounds changed their TE properties from *n*- to *p*-type with a dramatic increase in S, with $S > 100\mu$V/K at room temperature. These results suggest that nominally stoichiometric *M*CoSb compounds have intrinsic defects which make them *n*-type and the concentration of these defects depend on *M*. Sekimoto *et al.*[18] have also observed a similar change of sign in thermopower from negative to positive values when Sn content is increased in $ZrCoSn_xSb_{1-x}$ ($x \leq 0.15$) at higher temperatures. The highest ZT value(=0.45) has been obtained at 958 K with x=0.1.

On the theoretical side, there have been several studies of semiconducting half-Heusler compounds focusing mainly on their electronic structure such as the density of states (DOS), the physics of gap formation, and composition dependence of the band gap in quaternary systems, etc.[6–8,22–25] Most of these calculations have been carried out using

density functional theory (DFT) within local density approximation (LDA) or generalized gradient approximation (GGA). Hybridization between the d states of M and A atoms (in MASn or MASb systems) is found to play an important role in the formation of the band gap.[6,7] In addition to these band structure calculations, a theoretical survey of the electronic transport properties of a large number of semiconducting half-Heusler compounds was carried out by Yang *et al.*[25] They used the results of *ab-initio* band structure calculations and Boltzmann transport equation in conjunction with rigid band and constant relaxation time (τ) approximations to obtain σ and S in a large number of semiconducting HH compounds. They reported maximum power factors (obtained in unit of τ) and the corresponding optimal p- or n-type doping levels. These theoretical results can be used as a guide to find potentially good thermoelectric materials. In fact, they are being used to synthesize new quaternary HH compounds in order to enhance their TE properties.[26] However, due to the broad survey nature of their study, Yang *et al.* did not explore in detail the intricate relationships between the band structure, band degeneracy and the thermopower.

It is well known that changes in the carrier concentration and manipulation of the electronic structure in the neighborhood of the band gap and chemical potential can indeed increase the power factor of a TE material.[27] Therefore, understanding of not only the electronic structure but also how the subtle features of the band structure near the chemical potential affect transport properties is important to improve their TE performance. Nevertheless, until now there is no systematic study of how the differences in the band structures of different HH compounds affect their transport properties. Also from a theoretical perspective, before investigating more complex systems such as quaternaries involving half-Heusler compounds,[26] it is important to understand the TE behaviors with simple ternary compounds. This is the motivation for the present work. In this paper, we report the band structure and the transport properties of four HH compounds MASb where M=Hf or Zr, and A=Co or Ir and explore the interplay of their band structures and transport properties for different carrier concentrations. Since thermopower is less sensitive to the relaxation time (it is independent of the relaxation time when the latter is energy independent) we first discuss how it is affected by the non-parabolicity of the band structure and the band degeneracy. We then discuss the change in σ/τ and $S^2\sigma/\tau$ as a function of temperature, bringing out the effect of non-parabolic band structure on these transport related properties. We then compare our results with available experimental data.

The paper is arranged as follows. In Sec. II, we briefly describe the computational procedure and define the transport coefficients using the Boltzmann equation. We present our results and discussion in Sec. III. A summary is given in Sec. IV.

II. COMPUTATIONAL DETAILS

Scalar relativistic electronic structure calculations were carried out within DFT formalism using the projector augmented wave (PAW) methods[28] as implemented in VASP.[29] The Perdew-Burke-Ernzerhof (PBE) generalized gradient corrected exchange-correlation functionals are used.[30] An energy cutoff of 400 eV was used for the plane-wave expansion, with a total energy convergence of the order of 10^{-4} eV. A Fermi smearing factor of 0.026 eV is taken. We have used the FCC primitive unit cell with three atoms (M, A, Sb) and optimized the lattice parameters using total energy calculations. These lattice parameters are then used to calculate the electronic band structure and other properties. The accuracy of the band structure calculations using VASP is checked by comparing with those obtained from self-consistent full-potential linearized augmented plane-wave method[31] and PBE generalized gradient corrected exchange-correlation functionals using WIEN2k.[32] We find that both results agree very well with each other.

In the calculation of transport coefficients using Boltzmann transport theory, one needs to calculate the velocities, which are the derivatives of energy with respect to $\mathbf{k}$. To get more accurate values of the velocities, it is necessary to have dense $\mathbf{k}$-point mesh.[33–38] For this, we calculate the band structure using a $41 \times 41 \times 41$ Monkhorst-Pack $\mathbf{k}$-point sampling.[39] Since it is difficult to calculate the relaxation time τ associated with carrier-impurity and carrier-phonon scattering[38,40,41] using *ab-initio* band-structure results and since the band structures of these HH compounds cannot be approximated by simple parabolic (or nearly parabolic) band models, an energy-independent constant τ approximation was adopted in all our calculations. In this limit one can find out how the nonparabolic effects contribute to the energy dependence of the transport function (defined below) through both the density of states and carrier velocity. It should be pointed out that even with a constant τ approximation, it has been possible to successfully predict thermopower values, their temperature and carrier concentration dependence, and also trends in electrical conductivity for several materials.[42–44]

Within relaxation time approximation, tensors of electrical conductivity ($\sigma_{\alpha\beta}$), Seebeck coefficient ($S_{\alpha\beta}$), and electronic thermal conductivity ($\kappa_{el,\alpha\beta}$) at zero electric field $\mathbf{E}$ are given by

$$\sigma_{\alpha\beta}(T,\mu) = \frac{1}{\Omega}\int \sigma_{\alpha\beta}(\varepsilon)\left[-\frac{\partial f_0(T,\varepsilon,\mu)}{\partial \varepsilon}\right] d\varepsilon \tag{1}$$

$$\nu_{\alpha\beta}(T,\mu) = \frac{1}{eT\Omega\sigma_{\alpha\beta}(T,\mu)} \int \sigma_{\alpha\beta}(\varepsilon)(\varepsilon-\mu)\left[-\frac{\partial f_0(T,\varepsilon,\mu)}{\partial\varepsilon}\right] d\varepsilon \tag{2}$$

$$S_{ij} = (\sigma^{-1})_{\alpha i}\nu_{\alpha j} \tag{3}$$

$$\kappa_{el,\alpha\beta}(T,\mu) = \frac{1}{e^2T\Omega} \int \sigma_{\alpha\beta}(\varepsilon)(\varepsilon-\mu)^2\left[-\frac{\partial f_0(T,\varepsilon,\mu)}{\partial\varepsilon}\right] d\varepsilon \tag{4}$$

where e is the electronic charge, α and β are tensor indices, Ω, μ, and f_0 are the volume of unit cell, chemical potential, and Fermi-Dirac distribution function, respectively. In Eq. 3, repeated index implies summation over that index. In Eqs. 1, 2, and 4, the transport distribution function (TDF) tensor $\sigma_{\alpha\beta}(\varepsilon)$ is defined as

$$\sigma_{\alpha\beta}(\varepsilon) = \frac{e^2}{N}\sum_{i,\mathbf{k}} \tau \cdot v_\alpha(i,\mathbf{k}) \cdot v_\beta(i,\mathbf{k}) \cdot \frac{\delta(\varepsilon-\varepsilon_{i,\mathbf{k}})}{d\varepsilon} \tag{5}$$

where $\mathbf{k}$ and i are the wave vector and band index, respectively, and the summation is over the N $\mathbf{k}$-points sampled over the 1^{st} Brillouin zone (BZ). In the TDF tensor, $v_\alpha(i,\mathbf{k})(\alpha = x,y,z)$ is the α^{th} component of the group velocity $\mathbf{v}(i,\mathbf{k})$ of carriers in the band i with wave vector $\mathbf{k}$. The velocities can be obtained from the band dispersion using the relation

$$v_\alpha(i,\mathbf{k}) = \frac{1}{\hbar}\frac{\partial\varepsilon_{i,\mathbf{k}}}{\partial k_\alpha}. \tag{6}$$

For a cubic crystal, the different tensors become diagonal and all the diagonal elements are same. We have calculated the transport coefficients using BoltzTrap developed by Madsen and Singh.[35] These authors have employed an interpolation method to obtain accurate values for $\mathbf{v}(i,\mathbf{k})$ by fitting the band structure to analytical forms using a dense $\mathbf{k}$ mesh. Yang *et al.*[25] have also used the Boltzmann transport equation to calculate the transport coefficients in several HH compounds and their results agree very well with those obtained using BoltzTrap.

III. RESULTS AND DISCUSSION

A. Crystal structure and band gap

AMSb (A=Hf,Zr ; M=Co,Ir) crystallize in the cubic MgAgAs-type structure which can be regarded as four interpenetrating FCC sublattices: a lattice of A atoms and a lattice of Sb atoms, together forming a rock-salt structure, and a lattice of M atoms occupying the center of every other A_4Sb_4 cube formed by nearest neighbor A and Sb atoms, while the centers of the remaining A_4Sb_4 cubes are vacant. We have done total energy calculations to find the optimized lattice constants a for each system. The results are given in Table I along with calculated band gaps. Our lattice constants for ZrCoSb and HfCoSb agree well with experimental values of 6.0676 Å for ZrCoSb and 6.0383 Å for HfCoSb obtained by Sekimoto *et al.* at room temperature.[17] From the Table I we note that the lattice constants of Ir-compounds are about 5 % larger than those of the Co-compounds. Later, we will discuss how this difference affects the local bonding between different atoms and the resulting electronic structures. As we see, all the four compounds are narrow-band-gap semiconductors as predicted using the 18 valence electron count rule.[45,46] The largest band gap is seen in ZrIrSb, while HfIrSb gives the smallest band gap. The real band gaps are however likely to be larger due to the problems associated with GGA used in our calculations which underestimates the band gap in semiconductors.[47]

B. Electronic band structure

Band structures of the four compounds along the directions W-L-Γ-X-W-K of the 1^{st} BZ are shown in Fig. 1. While HfIrSb has a direct gap at the Γ point, ZrIrSb and the two Co systems, HfCoSb and ZrCoSb, have indirect

gaps between either the Γ point or the L point (valence band maxima, VBM) and the X point (conduction band minima, CBM). Indirect band gaps are found in several well known semiconducting half-Heusler systems containing Ni such as ZrNiSn and HfNiSn.[6] The difference between HfIrSb and the rest of the compounds is due to a low lying conduction band with minimum at the Γ point in this compound. A broad comparison of the band structures of the four systems shows pronounced differences between Co and Ir compounds (bands labeled 1-6 in Figs. 1 and 2; 1-3 are valence bands and 4-6 are conduction bands), but not between the Zr and Hf compounds, excepting for the above mentioned conduction band. We will now explain the physical origin of these observations.

Let us look at the valence bands first. The main differences between the Co and Ir compounds are (i) the separation between bands 1 and 2 at the Γ point, which is ∼3 eV in Ir compounds compared to ∼1.5 eV in Co compounds; and (ii) the VBM occurs at the Γ point in the Ir compounds and at the L point in the Co compounds. Although band 1 does not directly participate in transport, its position indirectly affects the transport mass associated with the band 2 and also the another flatter transport valence band 3, which is degenerate with band 2 at the Γ point. A detailed analysis of the orbital characters reveals that the band 1 is primarily the d-orbitals of Co/Ir whereas bands 2 and 3 come from hybridization of the d-orbitals of Zr/Hf and Co/Ir, as shown in Fig. 2 and also in the orbital projected density of states at the Γ point given in Fig. 3. We expect the transport effective mass of the holes near the VBM to be smaller in the Ir-compounds. We will discuss the effective mass values later in this paper. Since the VBM of Ir- and Co-compounds occur at different **k**-points, we expect that the nature of charge carriers contributing to transport is different. The other important characteristic features of the top valence bands that affect transport properties are the degeneracy and the number of equivalent points in the BZ. As shown in Fig. 2, the maximum at the Γ point is 3-fold degenerate whereas the one at the L point is 2-fold degenerate. However, there are 4 inequivalent L points compared to just 1 Γ-point in the BZ. As a result one expects the L-point holes to give much larger thermopower compared to the Γ-pocket holes.

Next, let us look at the conduction bands, labeled 4-6. In fact, bands 5 and 6 in the Co systems are very similar to those seen in ZrNiSn.[6,7] Band 5, which is the lowest conduction band (LCB) in these compounds, disperses rapidly downwards from the Γ point and flattens out as it approaches the X point, giving rise to a high effective electron mass along the X-Γ direction near the CBM. This band results from the hybridization between the Co d-states and the d-states of the neighboring Zr or Hf atoms and has strong Co d-character near the X point (See Figs. 2(a) and 2(b)). In Ir compounds the structure of the low lying conduction band is dramatically different. This can be understood by looking at the band 4. As shown in Fig. 2, the band 4 is a s-like state, coming mainly from Sb-s. In Co systems this band is quite high in energy. It does not hybridize with the low lying conduction band states which are primarily the d-orbitals of Co and Hf/Zr. In contrast, in Ir systems it hybridizes strongly with the band 5 along Γ-X and Γ-L directions but does not hybridize with band 6 along these directions for symmetry reasons. Thus there is a competition between the band 4 (minimum at the Γ point) and band 6 (minimum at the X point) to form the LCB. In HfIrSb band 4 wins and the minimum is at the Γ point whereas in ZrIrSb band 6 wins and the minimum is at the X point. This difference will show up in the thermopower of electron doped systems. As we will see later, although only one pocket near the energy minimum contributes to transport when the electron doping is small, both X and Γ pockets contribute to transport under sufficiently large doping.

To understand the origin of the above differences between Co and Ir systems further, we plot the orbital projected density of states at the Γ-point in Fig. 3. We see that there are 15 states (per spin) in the energy interval between -12.0 eV and +4.0 eV. They come from the 5 d-states of Co/Ir, 5 d-states of Zr/Hf, 3 p-states of Sb and 2 s-like states. The 2 s-like states consist of one deep bonding state (near -12.0 eV) and the corresponding antibonding state above the Fermi energy. They are formed out of 5s state of Sb and a linear combination s-states of Ir/Co and Zr/Hf. The position of the deep level near -12.0 eV does not change by more than 0.5 eV for the four systems. So we can use this level as a reference energy. The separation between the bonding and antibonding states is 12.5 eV for the Ir compounds and 14.5 eV for the Co compounds. As a result the antibonding s-state in the Co compounds is about 2 eV higher than in Ir compounds. One possible reason for this difference between Co and Ir compounds is the difference in their lattice constants. Due to the smaller lattice constant of the Co systems (∼0.25 Å smaller than the Ir systems), there is a stronger hybridization between different s orbitals leading to larger energy difference between the bonding and antibonding states. It results in the antibonding s-state lying ∼2 eV higher in Co- than in Ir-compounds. Another possible reason for seeing a low-lying antibonding s-state in the Ir systems is the smaller energy separation between the d and s levels in Ir systems (due to relativistic effect which lowers the s level) compared to the Co systems. From Fig. 3 we see that this d- s energy difference is ∼4.5 eV (in Ir) and ∼5.0 eV (in Co). So we believe that both the differences in hybridization and relativistic effects are responsible for the observed s-like state as the lowest conduction band state in the Ir compounds. In order to check whether the lowest conduction band is of s-symmetry one can do a NMR (Knight shift) measurement in n-doped HfIrSb. One should see a large hyperfine field through Fermi-contact interaction at different nuclear sites.[48] For similar doping levels, the other 3 systems, particularly ZrIrSb, should not have large contact hyperfine field. Also the optical spectrum should be very different between the Co and Ir compounds.

In Fig. 4, we show the density of states (DOS) near the band gap. As is well known, a rapid change in the DOS with energy is a good indicator of large thermopower. In the region of the valence bands, increase of the DOS near the band edge is much larger in the Co-compounds throughout the energy region as shown in the figure. This is related both to a larger effective mass and the multiplicity of the L point where the valence band maxima lies. In contrast, the Ir systems have a rather slowly varying DOS (due to the Γ point maxima and smaller effective mass, to be discussed later). Thus we expect the Co-compounds to show higher S for p-type doping. Similarly for n-type doping, Co systems should be better when the concentration is small whereas for larger doping Ir compounds should be as good or better. We will discuss this further in the following section.

C. Transport properties

We first note that half-Heusler compounds studied here show band gaps between 0.89 and 1.4 eV as given in Table I. As discussed by Singh, the magnitude of thermopower can decrease at high temperatures and low doping due to the compensation between holes and electrons when the band gap is small as seen, for example, in PbTe.[49] In this case it is necessary to critically examine the band gap obtained using LDA or GGA which underestimate the gap. However in the half-Heusler systems, this compensation effect is not pronounced because the band gaps are $\sim$1 eV or larger.

Electronic transport coefficients are calculated using the rigid band approximation (RBA).[37,44] According to the RBA, doping a system does not change its band structure but only the chemical potential. This approximation is widely used in theoretical calculations of transport properties of doped semiconductors and is a reasonably good approximation when the doping level is not very large.[37,38,42–44] In addition to the RBA we also assume the relaxation time τ to be energy independent. In this limit, the Seebeck coefficient is independent of τ and therefore any T-dependence of τ should not contribute to the T-dependence of S. Thus the T-dependence of S discussed in this paper should be reasonably realistic. However, for a proper understanding of the T-dependence of the electrical conductivity and the electronic contribution to the thermal conductivity, one needs to understand the different mechanisms (electron-phonon and electron-impurity scattering) contributing to τ, their relative strengths and their T-dependence.[38,40,41] Since we do not have a detailed theory of τ for the half-Heusler compounds at the present time we will calculate electronic conductivity and power factor in units of τ to see how they depend on carrier concentration. Any T- dependence they show will come from the non-parabolicity of their band structures and how it affects the transport velocities and the DOS.

In Fig. 5 we plot S as a function of carrier concentration in the four systems for T=300 K. In Figs. 6 and 7 we plot (a) the chemical potential (μ) (b) Seebeck coefficient (S) (c) electrical conductivity (σ/τ) and (d) power factor ($PF = S^2\sigma/\tau$) as a function of temperature (T) for two different carrier concentrations, n=2×10^{20}/cm^3 (left panel) and n=4×10^{21}/cm^3 (right panel) for p-doping (n_h) and n-doping (n_e), respectively. These concentrations can be achieved experimentally by substituting about 1 % and 20 % of a dopant assuming that each dopant donates one hole/electron and all the doped holes appear as charge carriers. The zero of energy has been chosen at the middle of the band gap. To understand the differences between the transport properties of the different compounds, we show the chemical potential at 300 K in Fig. 8 for the two different concentrations, both for p- and n-type dopings. We now discuss the p- and n-doping cases, separately.

1. p-type

We see in Fig. 5(a) that S decreases with increase in carrier concentration n_h as expected. Larger S values are seen in Co-compounds for the entire range of n_h shown in the figure. This is consistent with the observed rapid change in the DOS with decreasing energy (Fig. 4). For Ir-compounds, however, the change of DOS is small in the region near the band edge. This results in S values nearly half of those in Co-compounds at low concentrations, but for higher concentrations the difference between Co and Ir systems become small where the DOS in all of them change rapidly.

At low carrier concentration (Fig. 6 (left panel)), the three curves for μ which are close to each other are for HfCoSb, ZrCoSb and HfIrSb, where their band gaps are within $\sim$10 % of each other from 1 eV (see Table I). The isolated curve is for ZrIrSb which has a much larger band gap of 1.4 eV. As expected, for hole doping μ increases with increasing T, moving towards the band gap. It is nearly T-independent below 100 K and its values are consistent with differences in the band gap values. The change of μ with T is slightly larger for the Co-systems, which is consistent with both the larger valence band effective mass for the Co compounds (see Table II) and the near degeneracy of the energy bands near the Γ and the L points. The band structures of all the four compounds are quite similar near the top of the valence band region in terms of the degeneracy and overall shape. However, in the the Co compounds the valence band maximum is at the L point whereas in the Ir compounds it is at the Γ point. Especially at low concentrations, both the L and Γ pocket holes contribute in HfCoSb. In contrast, only L pocket holes contribute in ZrCoSb and Γ

pocket holes in HfIrSb and ZrIrSb. These differences indeed show up in the overall magnitude of S (larger for the Co compounds). We also observe that the T-dependence of S and PF in Co compounds is stronger at low temperatures but weaker at high temperatures.

We find that at high T the values of the PF are more than a factor of 2 larger for the higher concentration. This comes from an increase in σ/τ by a factor of 10 (basically due to the increase in carrier concentration) and decrease in S by a factor of 2 in going from smaller to the larger carrier concentration. For both the concentrations, Co compounds give similar S values but larger than those for the Ir compounds. In HfCoSb, S is 90μV/K at room temperature and reaches 180 μV/K at 1000 K for the high concentration. We find an interesting behavior in these Co-systems. According to Pisarenko relation[50], S decreases with increasing n. Conversely, σ increases with increasing n. Thus, one expects to see an increase in S along with a decrease in σ when n decreases. This is seen in Ir-compounds, but in Co-compounds this is violated, a system with larger S also gives higher σ, indicating that the simple Pisarenko relation does not be hold. This anomalous behavior comes from the fact that in Co compounds both Γ and L pocket holes contribute to the transport.

At the lower concentration (n_h=2$\times 10^{20}$/cm^3) and high T (>650 K), ZrIrSb gives the highest PF caused by a rapid increase of S and a rather large σ/τ. Another interesting observation is that at this lower concentration, the PF of Co-compounds tend to saturate at high T, while those for Ir-compounds increase continuously with T. Thus, for this lower concentration of holes, the Ir-compounds should be better thermoelectrics at high T. At the high concentration, the Co compounds do better. In fact, the highest PF ($\sim 2\times 10^{16}\mu$W cm^{-1} K^{-2} s^{-1}) at 1000 K is obtained in HfCoSb for n_h=4 $\times$ 10^{21}/cm^3.

2. n-type

Seebeck coefficient (magnitudes) of the Co-compounds are larger at low n_e but smaller at higher n_e (Fig. 5(b)). Thus for smaller n-doping the Co compounds are better thermoelectrics, while the Ir compounds becomes better for larger n-doping. This behavior can be understood in terms of the energy dependence of the change of DOS for the conduction band near the band edge. For the Co compounds, as shown in Fig. 4, it is much larger near the band edge (hence effective at low n_e) but smaller at higher energies (effective at high n_e). This is opposite in the Ir compounds.

In Fig. 7 (left panel), for the smaller concentration, we see that the chemical potential decrease more rapidly with T. Both the Co compounds behave similarly and the difference is due to the small difference in their band gaps (1.06 eV for ZrCoSb and 1.13 eV for HfCoSb). A rather unusual behavior is seen in the case of the two Ir compounds. Although ZrIrSb and HfIrSb have a large difference in their band gaps i.e. 1.40 eV for the former and 0.89 eV for the latter, the values of the chemical potential at low T are almost identical. This can be understood by looking at their conduction band structures (Fig. 2). HfIrSb has a smaller gap but its conduction band is the s-band (minimum at the Γ point) with smaller effective mass (smaller density of states), whereas ZrIrSb has a larger gap but its conduction band is the d-band of Zr (minimum at the X point) with a large effective mass (Table II). The larger band gap in the Zr case is compensated by a smaller Fermi energy as measured from the bottom of the conduction band minimum (0.38 eV for the Hf system and 0.12 eV for the Zr system). This difference 0.26 eV is nearly equal to half of the difference in their band gaps, 0.51 eV. At the high concentration, this difference in the Fermi energies is $\sim$ 0.48 eV and as a result the chemical potentials are quite different (see Fig. 8 (right panel)).

For the smaller carrier concentration, the two cobalt compounds give large thermopowers for 100 K $\leq T \leq$ 1000 K. This is due to the large effective mass of the electrons associated with the carriers at the X point (see Table II). Both the Ir compounds start out with a smaller S values (magnitude) at 100 K due to small effective mass of the carriers at the X point for ZrIrSb and the Γ point for HfIrSb. In the ZrIrSb the magnitude of S increases dramatically and becomes closer to the value of the Co systems at 1000 K. This is due to the presence of another conduction band with the minimum at the Γ point which is 0.12 eV above the Fermi energy, resulting in multi-pocket contribution in transport. In the Hf case no such band exists and S behaves like that for a single nondegenerate band. Our calculations clearly point out the inadequacy of simple nondegenerate single band models to describe the T-dependence of thermopower in these half-Heusler systems. For higher concentration (Fig. 8 (right panel)), ZrIrSb gives the best thermopower value due to the contribution of multiple bands with multiple degeneracy. At this concentration the values of σ/τ are within 20 % of each other and the largest power factor is given by ZrIrSb with 1.5 $\times$ 10$^{16}\mu$W cm^{-1} K^{-2} s^{-1} at 1000 K.

Since we have assumed a constant relaxation time, the electrical conductivity is expected to show T-independent behavior for parabolic bands. However, we observe an increase of σ/τ with increasing temperature in electron-doped Co-compounds. This can be understood with the change of effective mass due to the non-parabolic band structure. It can be seen in Fig. 8 (right panel) that the effective mass decreases by moving away from the band edge. Thus at high temperatures, lighter mass electrons contribute to σ/τ resulting in the increase of σ/τ. More interesting behavior is seen in ZrIrSb, where σ/τ decreases rapidly with increasing T. This is because at high temperature one more band

contributes to the σ/τ, in addition to the CBM at X. Both the X- and Γ-pocket electrons have larger effective mass and we attribute the decrease of σ/τ to the multi-band as well as multi-pocket contributions. These calculations suggest that unusual band structures can give rise to strong T-dependence of electrical conductivity.

D. Comparison with experiments

Since we do not have the scattering time, we will not discuss the electrical conductivity any further but focus on the comparison between theoretical and experimental S values. Since S is weakly dependent on τ, comparison of S values is more meaningful. We will discuss the results for ZrCoSb since only this system has been studied experimentally. There are two measurements, one at low temperatures (below 320 K) for both p- and n-type dopings by Xia *et al.*[14], and the other at high temperatures (above 320 K) for only p-type doping by Sekimoto *et al.*[18] In both cases, it is seen that nominally stoichiometric ZrCoSb is n-type, most likely due to intrinsic defects. Replacing Sb by Sn makes it p-type and replacing Co by Pt makes it n-type. In Fig. 9, we plot S for 10 % p- and n-dopings. Our value of S is 113 μV/K at room temperature which is about 13 % lower than the experimental value (130 μV/K) for the p-type. For the n-doping, the theoretical value (-74 μV/K) is about 23 % lower than the experimental value (-101 μV/K) in their magnitude. At higher temperatures the difference between experiment and theory is even larger ($\sim 30\mu$V/K) but smaller percentage-wise. One possible source of this discrepancy could be due to the difference in the carrier concentrations used in our calculations (for a given doping of 10 %) and the actual concentrations in the samples. It is known experimentally that all dopants do not contribute carriers because some of the dopant electrons are localized compensating for intrinsic defects. Thus actual carrier concentration can be different form what one calculates form the nominal dopant concentration. In contrast, theoretical studies assume that all dopants contribute to carriers. Consequently, a smaller value of the actual concentration in the experiment can account for the observed larger magnitude of S. Other possible sources are the contribution from phonon drag effect at low temperatures (below the Debye temperature) and T-dependence of band structure parameters at high temperatures.

IV. SUMMARY

In summary, we have discussed the band structures of four half-Heusler semiconductors (Zr,Hf)(Co,Ir)Sb of current thermoelectric interest obtained using *ab initio* density functional methods within GGA. Using the calculated band structures and Boltzmann transport theory (in RBA and constant relaxation time τ) we have calculated thermopower S, electrical conductivity σ and power factor $S^2\sigma$ (in unit of τ), for both p- and n-dopings at two different carrier concentrations ($n = 2 \times 10^{20}/\text{cm}^3$ and $4 \times 10^{21}/\text{cm}^3$). Since τ depends on different scattering mechanisms (electron-impurity, electron-electron, and electron-phonon) whose relative importance change with temperature and carrier concentration (see Refs. 38,40), a quantitative study of τ is difficult, particularly using the results of *ab initio* band structure calculations. For this reason we have reported σ/τ and the power factor $S^2\sigma/\tau$ in this paper. These scaled quantities reflect the effect of the electronic structure on transport coefficients coming from carrier velocities (effective mass), band degeneracy and the density of states.

There are several interesting aspects of the electronic structure of these four compounds that we would like to emphasize. In Co compounds, the VBM is at the L point and is primarily of Co-d character, hybridized with Zr/Hf-d states. This is different from ZrNiSn where the VBM is at the Γ point.[7] In addition, in HfCoSb the VBM at the L point is nearly degenerate with another maximum at the Γ point. Since there are four inequivalent L points and only one Γ point in the BZ, a system with contribution from L pocket to the transport properties is likely to have larger thermopower than the others. In fact in Co compounds both the maxima contribute to S making it a very good p-type thermoelectric. In the Ir compounds, the valence band structure is closer to what is seen in the Ni compounds,[7] i.e. the VBM is at the Γ point and the maximum at the L point has lower energy. So the Γ-point holes contribute mostly to charge and energy transport in the p-doped case.

The Co compounds show similar conduction band structure to the well known compound ZrNiSn.[6,7] The conduction band minimum (CBM) is at the X point and the states near this minimum show predominantly Co-d character (similar to Ni-d character in ZrNiSn) coming from the strong hybridization between the Co-d and Zr(Hf) d-states. These electron carriers have large effective masses (Table II) and give large thermopower. The major difference between the Ir and Co (also Ni) is in the conduction band transport. In the Ir compounds, the low lying antibonding s-state hybridizing with the Zr(Hf) d-states gives rise to the CBM in HfIrSb and a nearly degenerate CBM in ZrIrSb at the Γ point, not at the X point. Unfortunately this difference along with lighter electron effective mass gives smaller (in magnitude) electron thermopower in the Ir compound for small carrier concentration (n_e=$2 \times 10^{20}/\text{cm}^3$). However when the carrier concentration is increased (n_e=$4 \times 10^{21}/\text{cm}^3$), both Γ and X pockets contribute resulting in high

S in the Ir compounds. Particularly in ZrIrSb, in addition to major contributions from two bands having three inequivalent X points, contribution from Γ- and K-pockets results in large thermopower at high temperatures.

Nearly same value of S in different Co-compounds as seen in Fig. 7 can also be explained in terms of their band structures. The shape of the lowest conduction band which is the only band contributing to transport is almost the same for both of HfCoSb and ZrCoSb (See Fig. 8 (left panel)), resulting in similar effective mass and same symmetry-pocket contributions. Higher value of S in ZrIrSb compared to HfIrSb at low concentration (Fig. 7) is due to a flatter conduction band and 3 inequivalent X-pocket contributions in the former compared to Γ-pocket contribution with smaller effective mass in the later.

We have examined the effect of spin-orbit interaction (SOI) on the band structures of these compounds. We found that in general the removal of degeneracy due to SOI leads to a reduction in the magnitude of the thermopower in these systems. In the Co compounds we found that the changes in the band structures and transport properties were negligible (thermopower changes by less than 0.5 %). In the Ir compounds, however, splitting of the degeneracy of the VBM (associated with Zr-t_{2g}-like states) was found to be substantial leading to a reduction in the thermopower ($\sim$ 10 %). Nevertheless, the order of magnitude of S and its T and concentration dependence does not change when SOI is included.

We conclude by noting that *ab initio* band structure calculations have been extremely helpful in understanding the subtle differences in the transport properties of different semiconducting half-Heusler systems.[25,49,51] The next step in the research vis-à-vis these half-Heusler systems should be in two directions; first to understand the temperature, concentration, and the energy dependence of the relaxation time τ and how it affects the electrical conductivity and the power factor, second to check the adequacy of the rigid band approximation in the calculation of transport coefficients. Many half-Heusler systems show large thermopower at relatively large carrier concentrations $\sim 10^{21}/\mathrm{cm}^3$. At these doping levels, one should re-examine whether the band structure of the host system gets perturbed by the dopant.

Acknowledgments

MS acknowledge financial support from DARPA (Contract No. HR0011-08-1-0084) awarded to the Advanced Materials Institute (AMRI). This research partly used resources of the National Energy Research Scientific Computing Center, which is supported by the Office of Science of the U.S. Department of Energy under Contract No. DE-AC02-05CH11231.

[1] G. A. Slack, in *Proceedings of Thermoelectric Materials-New Directions and Approaches*, Pittsburgh, PA, 1997, edited by T. M. Tritt, M. G. Kanatzidis, H. B. Lyon, Jr., G. D. Mahan (Materials Research Society, Pittsburgh, PA, 1997), Vol. **478**, p. 47.
[2] G. J. Snyder and E. S. Toberer, Nat. Mater. **7**, 105 (2008).
[3] W. Jeitschko, Metall. Trans. A **1**, 3159 (1996).
[4] F. G. Aliev, V. V. Moshchalkov, V. V. Kozyrkov, R. V. Skolozdra, and A. I. Belogorokhov, Z. Phys. B **75**, 167 (1989).
[5] F. G. Aliev, V. V. Kozyrkov, V. V. Moshchalkov, R. V. Skolozdra, and K. Durczewski, Z. Phys. B **80**, 353 (1990).
[6] S. Öğüt and K. M. Rabe, Phys. Rev. B **51**, 10443 (1995).
[7] P. Larson, S. D. Mahanti, S. Sportouch, and M. G. Kanatzidis, Phys. Rev. B **59**, 15660 (1999).
[8] B. R. K. Nanda and I. Dasgupta, J. Phys.: Condens. Matter **15**, 7307 (2003).
[9] C. Uher, S. Hu, J. Yang, G. P. Meisner, and D. T. Merelli, *Proceedings of 16th International Conference on Thermoelectrics* (IEEE, Piscataway, NJ, 1997) p. 485.
[10] C. Uher, J. Yang, S. Hu, D. T. Morelli, and G. P. Meisner, Phys. Rev. B **59**, 8615 (1999).
[11] H. Hohl, A. P. Ramirez, C. Goldmann, G. Ernst, B. Wolfing, and E. Bucher, J. Phys.: Condens. Matter **11**, 1697 (1999).
[12] K. Mastronardi, D. Young, C. C. Wang, P. Khalifah, R. J. Cava, and A. P. Ramirez, Appl. Phys. Lett. **74**, 1415 (1999).
[13] S. R. Culp, S. J. Poon, N. Hickman, T. M. Tritt, and J. Blumm, Appl. Phys. Lett. **88**, 042106 (2006).
[14] Y. Xia, S. Bhattacharya, V. Ponnambalam, A. L. Pope, S. J. Poon, and T. M. Tritt, J. Appl. Phys. **88**, 1952 (2000).
[15] Y. Xia, V. Ponnambalam, S. Bhattacharya, A. L. Pope, S. J. Poon, and T. M. Tritt, J. Phys.: Condens. Matter **13**, 77 (2001).
[16] M. Zhou, C, Feng, L. Chem, and X. Huang, J. Alloys Compd. **391**, 194 (2005).
[17] T. Sekimoto, K. Kurosaki, H. Muta, and S. Yamanaka, *2005 24th International Conference on Thermoelectrics* (IEEE Cat. No. 05TH8854, 2005) p. 335.
[18] T. Sekimoto, K. Kurosaki, H. Muta, and S. Yamanaka, Jpn. J. Appl. Phys. **46**, L673 (2007).
[19] S. R. Culp, J. W. Simonson, S. J. Poon, V. Ponnambalam, J. Edwards, and T. M. Tritt, Appl. Phys. Lett. **93**, 022105 (2008).
[20] W. Xie, Q. Jin, and X. Tang, J. Appl. Phys. **103**, 043711 (2008).
[21] P. Qiu, X. Huang, X. Chen, and L. Chen, J. Appl. Phys. **106**, 103703 (2009).
[22] L. Chaput, J. Tobola, P. Pécheur, and H. Scherrer, Phys. Rev. B **73**, 045121 (2006).
[23] L. P. Romaka, M. G. Shelyapina, Y. V. Stadnyk, D. Fruchart, E. K. Hlil, V. A. Romaka, J. Alloy. Compd. **416**, 46 (2006).
[24] J. Tobola, L. Jodin, P. Pécheur, and G. Venturini, Scherrer, J. Alloy. Compd. **383**, 328 (2004).
[25] J. Yang, H. Li, T. Wu, W. Zhang, L. Chen, and J. Yang, Adv. Funct. Mater. **18**, 2880 (2008).
[26] M. A. Verges, P. J. Schilling, J. D. Germond, P. Upadhyay, W. K. Miller, N. J. Takas, P. F. P. Poudeu, in *Thermoelectric Materials - Growth, Properties, Novel Characterization Methods, and Applications*, edited by H.L. Tuller, J.D. Baniecki, G.J. Snyder, J.A. Malen (Mater. Res. Soc. Symp. Proc. Vol. **1267**, Warrendale, PA, 2010), DD05-23.
[27] J. O. Sofo and G. D. Mahan, Phys. Rev. B **49**, 4565 (1994).
[28] G. Kresse and D. Joubert, Phys. Rev. B 59, 1758 (1999); P. E. Blöchl, Phys. Rev. B **50**, 17953 (1994).
[29] G. Kresse and J. Hafner, Phys. Rev. B 47, 558 (1993); G. Kresse and J. Furthmüller, Comput. Mater. Sci. 6, 15 (1996); G. Kresse and J. Furthmüller, Phys. Rev. B 54, 11169 (1996); see website: http://cms.mpi.univie.ac.at/vasp/.
[30] J. P. Perdew, K. Burke, and M. Ernzerhof, Phys. Rev. Lett. **77**, 3865 (1996).
[31] D. J. Singh, *Planewaves, Pseudopotentials, and the LAPW Methods* (Kluwer Academic, Boston, 1994).
[32] P. Blaha, K. Schwarz, G. Madsen, D. Kvasnicka, and J. Luitz, *WIEN2k, An Augmented Plane-wave+Local Orbitals Program for Calculating Crystal Properties, edited by Karlheinz Schwarz* (Technische Universitat Wien, Austria, 2001)
[33] D. J. Singh, Semiconduc. Semimet. **70**, 125 (2001).
[34] T. J. Scheidemantel, C. Ambrosch-Draxl, T. Thonhauser, J. V. Badding, and J. O. Sofo, Phys. Rev. B **68**, 125210 (2003).
[35] G. K. H. Madsen, D. J. Singh, Comput. Phys. Commun. **175**, 67 (2006).
[36] G. K. H. Madsen, J. Am. Chem. Soc. **128**, 12140 (2006).
[37] L. Chaput, P. Pécheur, J. Tobola, and H. Scherrer, Phys. Rev. B **72**, 085126 (2005).
[38] D. I. Bilc, S. D. Mahanti, and M. G. Kanatzidis, Phys. Rev. B **74**, 125202 (2006).
[39] H. J. Monkhorst, J. D. Pack, Phys. Rev. B **13**, 5188 (1976).
[40] Salameh Ahmad and S. D. Mahanti, Phys. Rev. B **81**, 165203 (2010).
[41] Bao-Ling Huang and Massoud Kaviany, Phys. Rev. B **77**, 125209 (2008).
[42] J. M. Ziman, *Electrons and Phonons: Theory of Transport Phenomena in Solids* (Oxford University Press, London, UK 1960).
[43] B. R. Nag, *Electron Transport in Compound Semiconductors* (Springer-Verlag, Berlin, Germany 1980).
[44] L. Jodin, J. Tobola, P. Pécheur, H. Scherrer, and S. Kaprzyk, Phys. Rev. B **70**, 184207 (2004).
[45] J. Tobola, S. Kaprzyk, R. V. Skolozdra, and M. A. Kouacou, J. Phys.: Condens. Matter **10**, 1013 (1998).
[46] J. Tobola and J. Pierre, J. Alloys Compd. **296**, 243 (2000).
[47] W. G. Aulbur, L. Jönsson, and J. W. Wilkins, Solid State Phys. **54**, 1 (1999).
[48] W. D. Knight, in *Solid State Physics*, (Academic Press Inc., New York (1956), vol. **2**, p. 93.
[49] David J. Singh, Phys. Rev. B **81**, 195217 (2010).
[50] A. F. Ioffe, *Physics of Semiconductors* (Academic, New York, 1960).

[51] L. Chaput, J. Tobola, P. Pécheur, and H. Scherrer, Phys. Rev. B **73**, 045121 (2006).

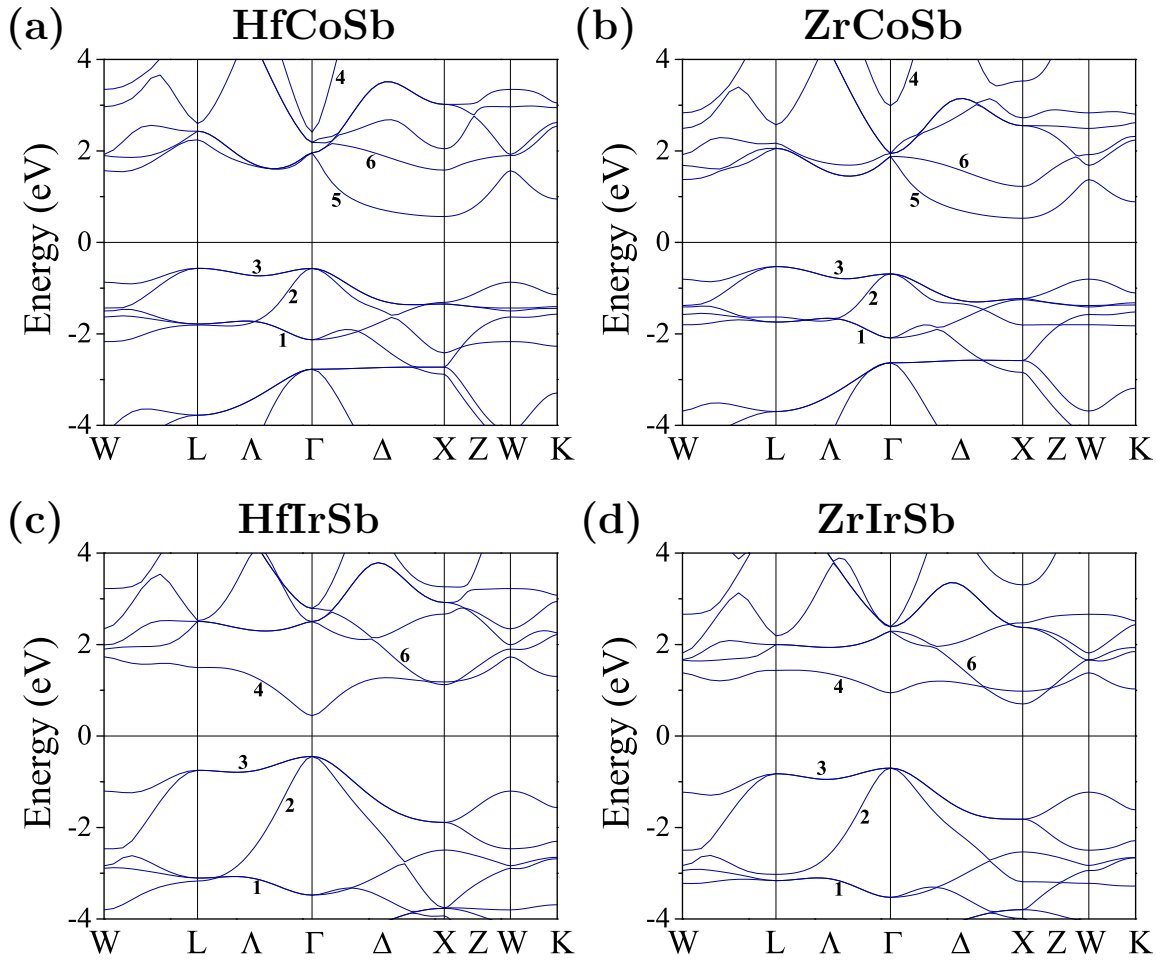

FIG. 1: The band structure near the Fermi energy for (a) HfCoSb, (b) ZrCoSb, (c) HfIrSb, and (d) ZrIrSb along W-L-Γ-X-W-K. The Fermi level is set to be zero energy.

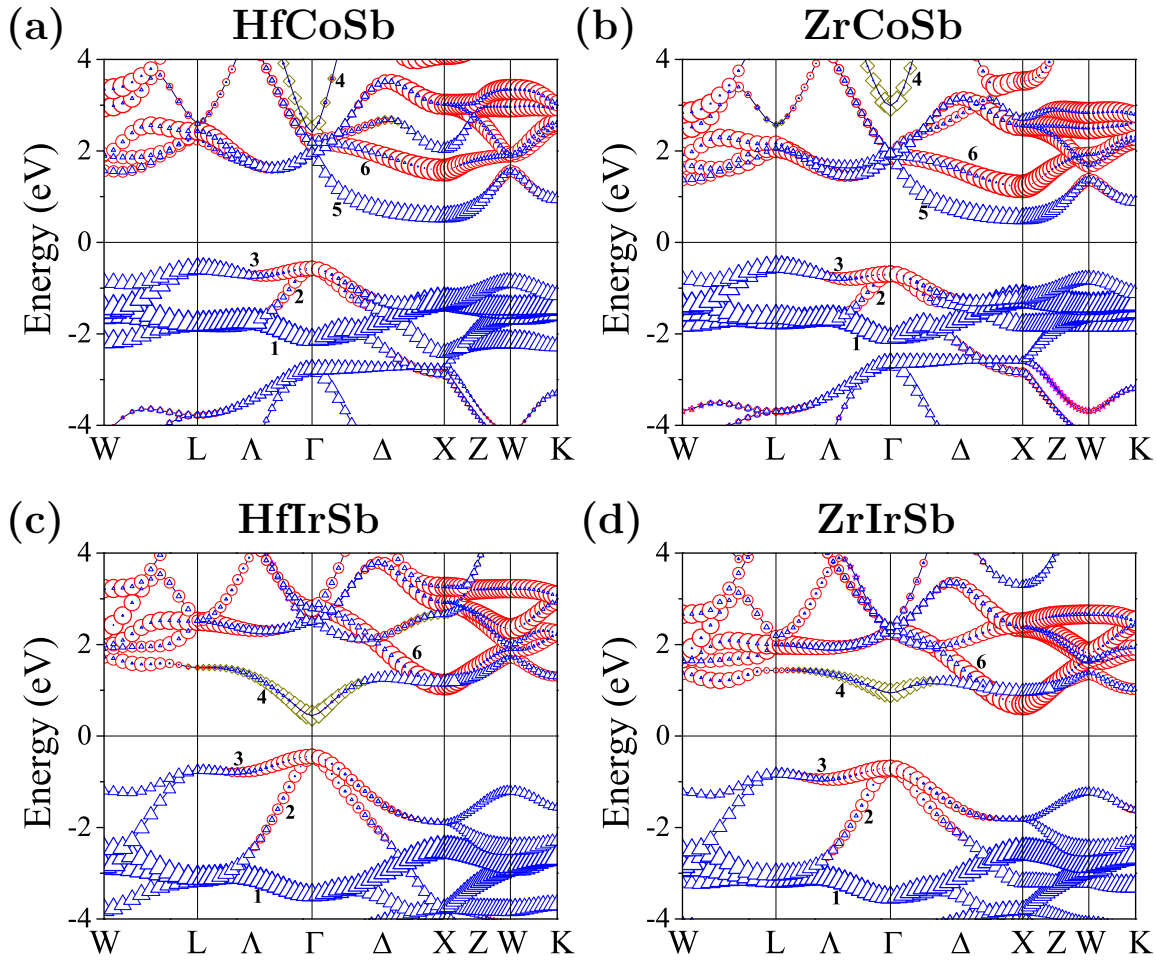

FIG. 2: The contribution of each atoms in the band structure of (Hf,Zr)(Co,Ir)Sb compounds: red circles for d-orbital of Hf/Zr, blue triangles for d-orbital of Co/Ir, pink stars for p-orbital of Sb, and green diamonds for s-orbital of Sb. The size of the symbols represents the strength of the contribution. The Fermi level is set to be zero energy.

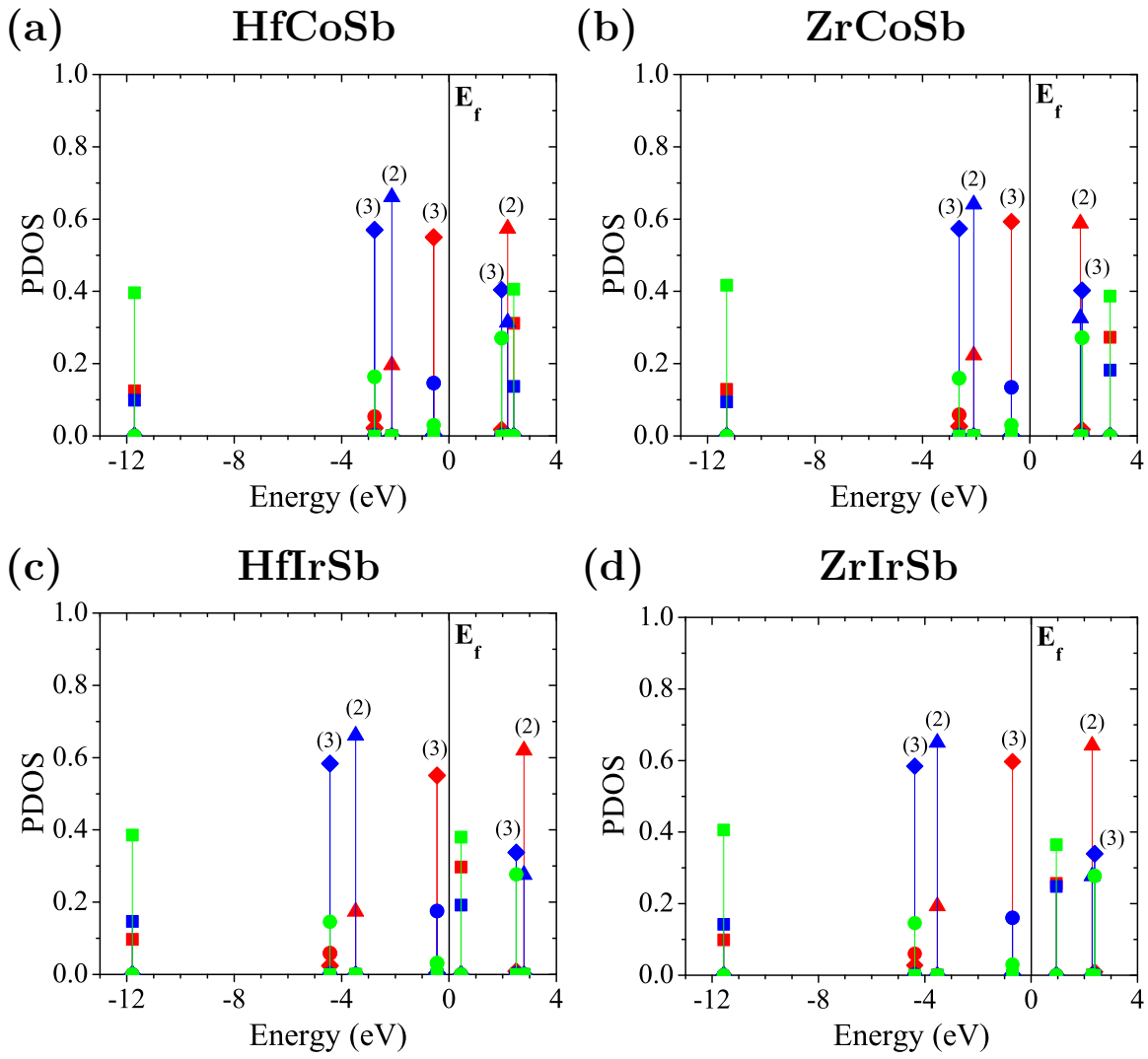

FIG. 3: The projected density of states (PDOS) as a function of energy. The value in parentheses is the number of degeneracy. E_f denotes the Fermi level. Each symbol represents different orbitals: square for s-orbital, circle for p-orbital, triangle for e_g-orbital, and diamond for t_{2g}-orbital. Each color represents different element: red for Hf/Zr, blue for Co/Ir, and green for Sb.

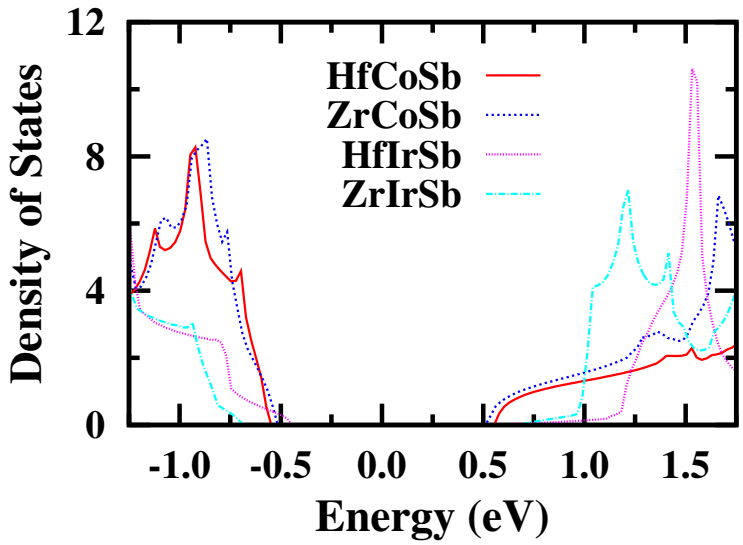

FIG. 4: The density of states (PDOS) with the Fermi energy to be zero.

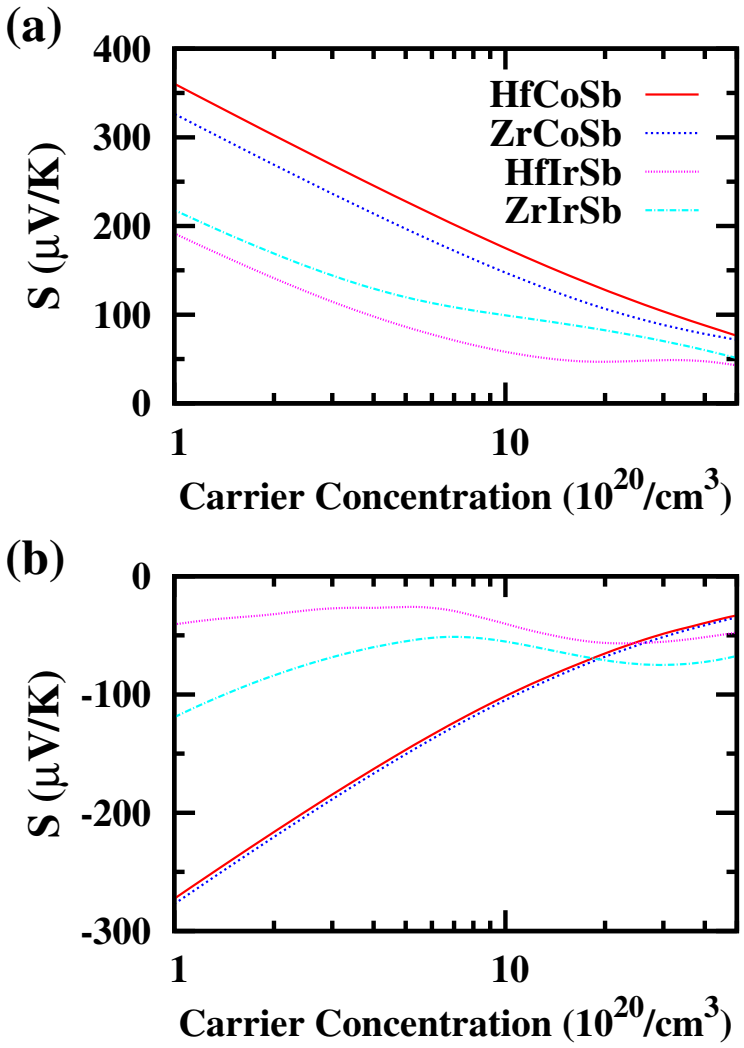

FIG. 5: Seebeck coefficient as a function of carrier concentration at 300 K for (a) hole-doping and (b) electron-doping.

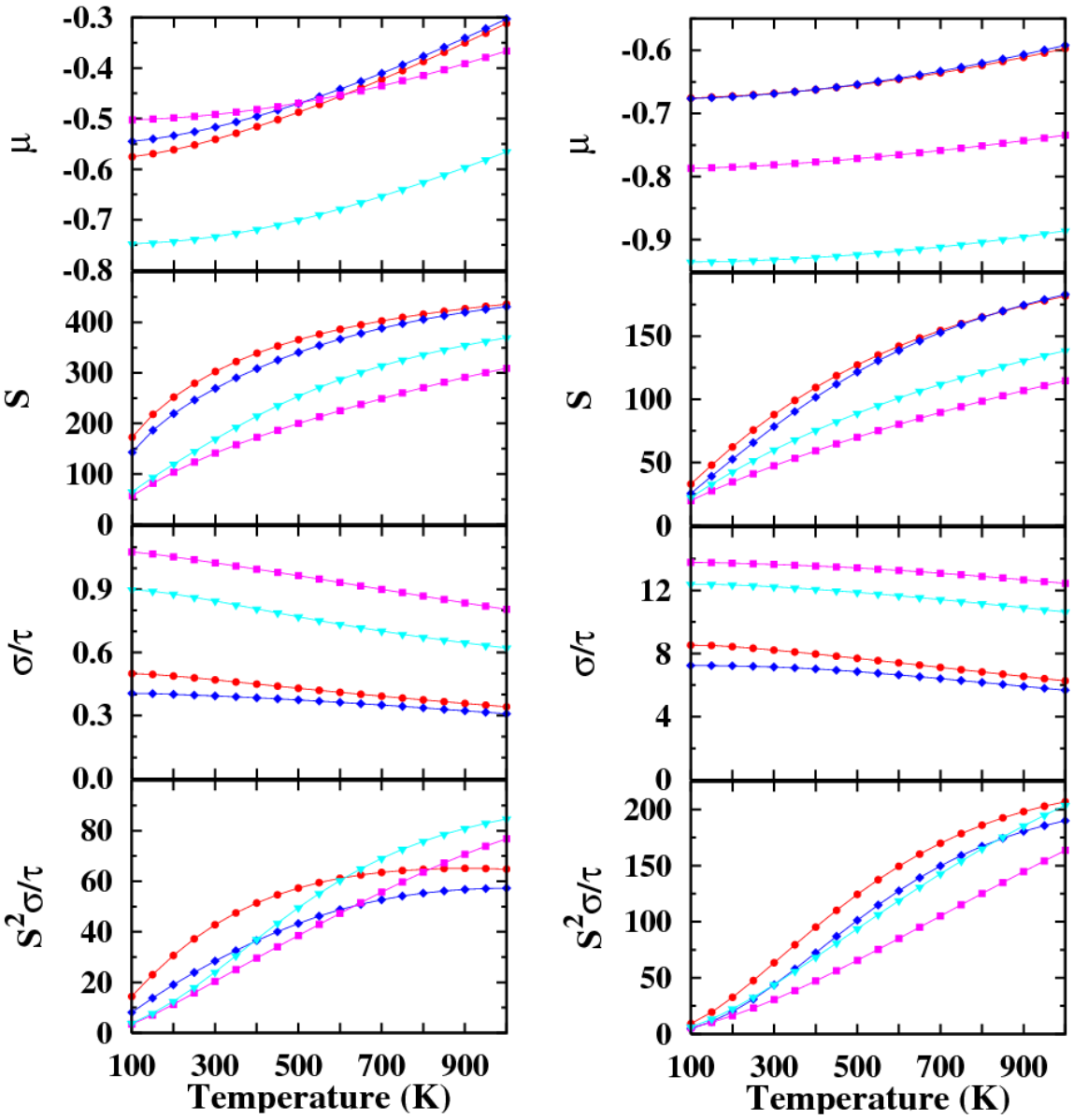

FIG. 6: Transport properties for HfCoSb (red circle), ZrCoSb (blue diamond), HfIrSb (pink square), and ZrIrSb (sky blue triangle) as a function of temperature at the hole-concentration n_h=2 × 10^{20}/cm^3(left panel) and n_h=4 × 10^{21}/cm^3 (right panel). The units for μ, S, σ/τ, and $S^2\sigma/\tau$ are eV, μV/K, $10^{17}\Omega^{-1}$cm^{-1}s^{-1}, and $10^{14}\mu$W cm^{-1} K^{-2} s^{-1}, respectively.

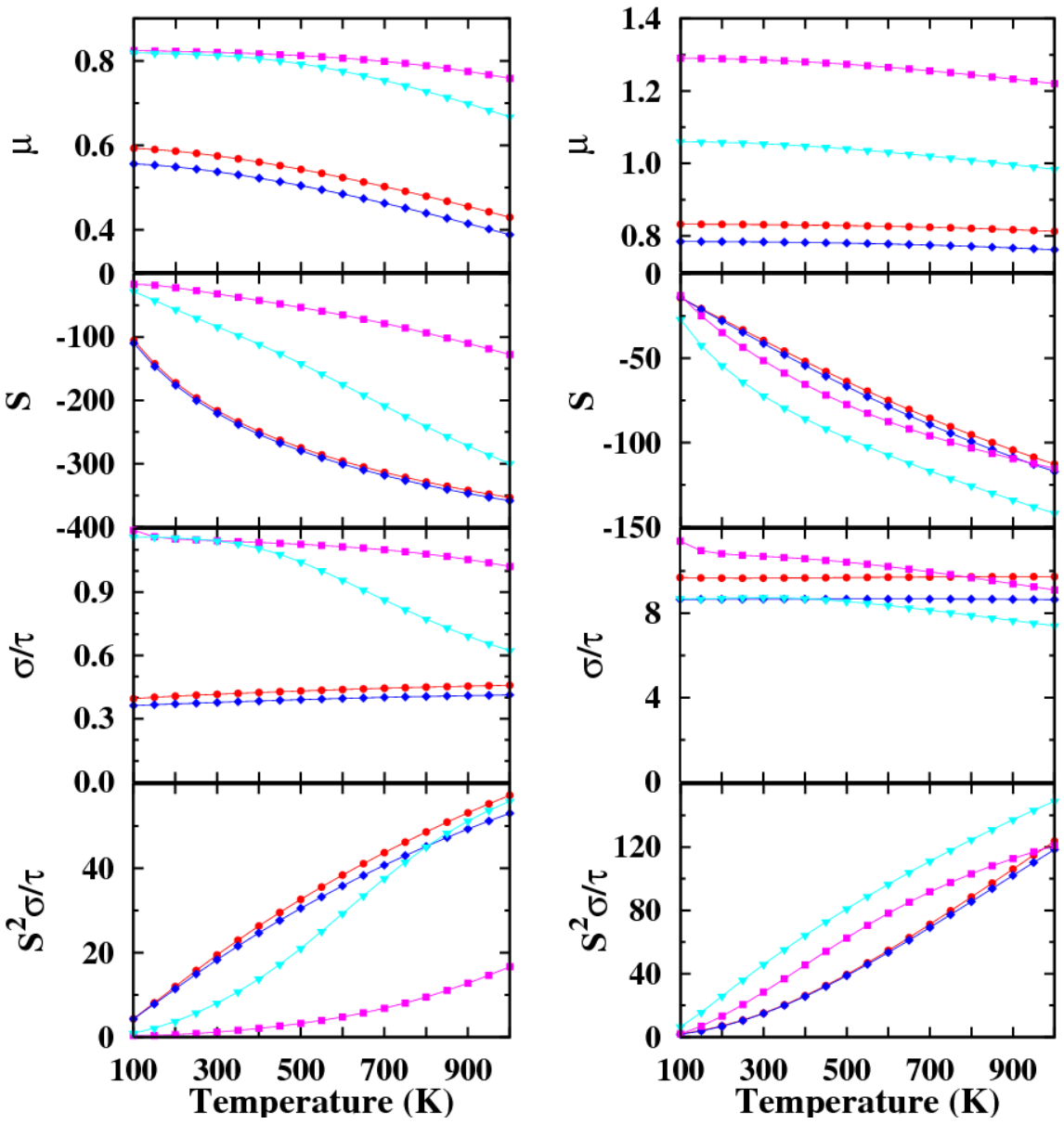

FIG. 7: Transport properties for HfCoSb (red circle), ZrCoSb (blue diamond), HfIrSb (pink square), and ZrIrSb (sky blue triangle) as a function of temperature at the hole-concentration n_e=2×10^{20}/cm^3(left panel) and n_e=4×10^{21}/cm^3 (right panel). The units for μ, S, σ/τ, and $S^2\sigma/\tau$ are eV, μV/K, $10^{17}\Omega^{-1}$cm^{-1}s^{-1}, and $10^{14}\mu$W cm^{-1} K^{-2} s^{-1}, respectively.

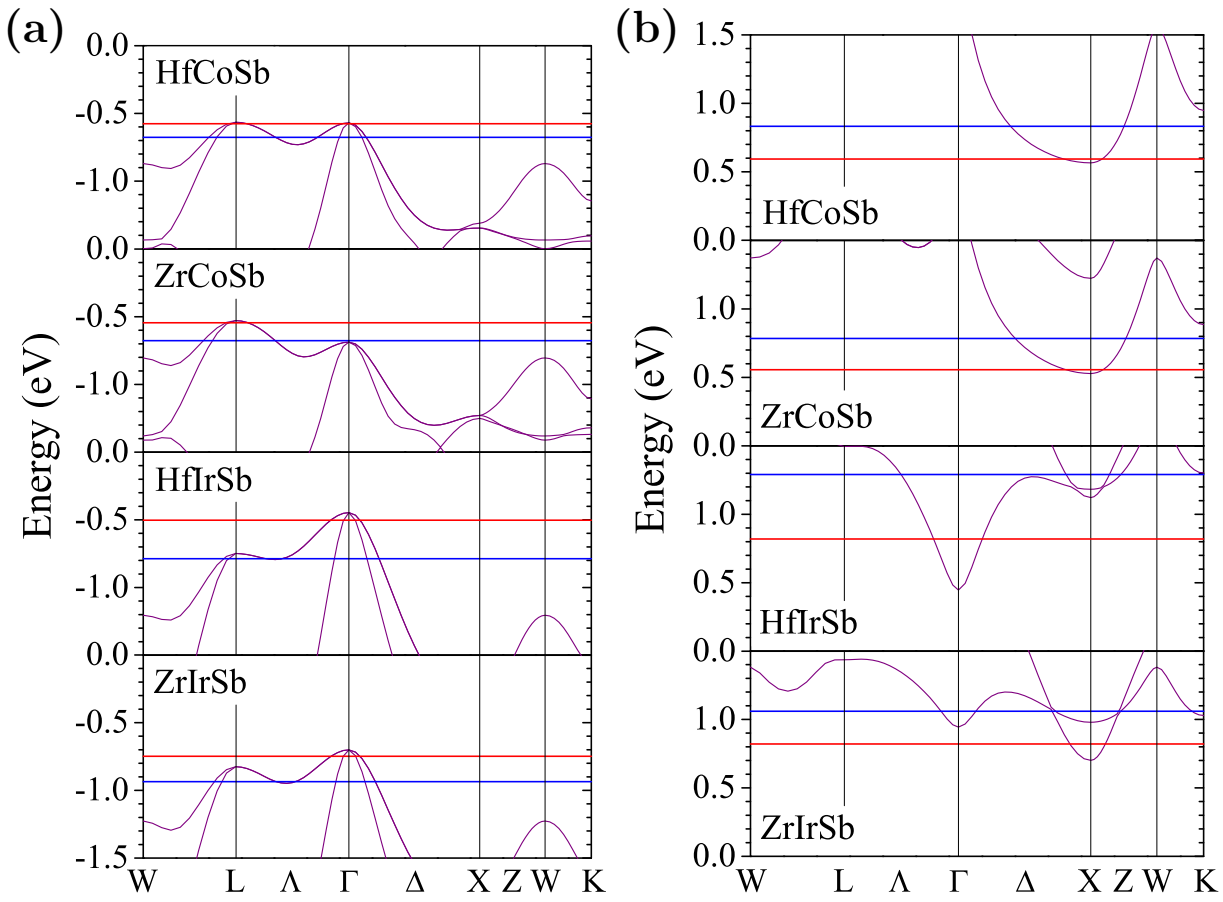

FIG. 8: Fermi level change at the carrier concentration of n=2×10^{20}/cm^3 (red lines) and n=4×10^{21}/cm^3 (blue lines) by (a) hole-doping and (b) electron-doping.

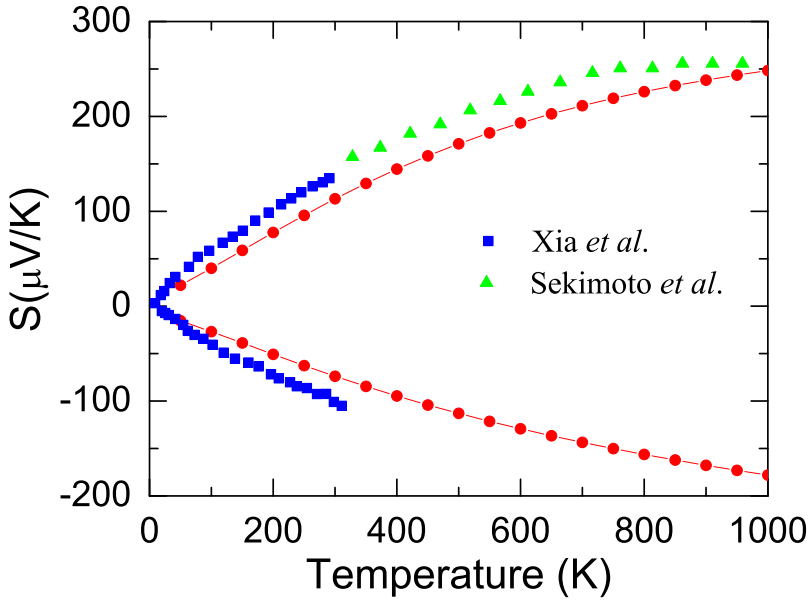

FIG. 9: Seebeck coefficient with 10 % doping in ZrCoSb. Theoretical values are shown with lines and experimental data with rectangles for low temperatures by Xia *et al.* [Ref. 14] and triangles for high temperatures by Sekimoto *et al.* [Ref. 18].

TABLE I: The optimized lattice constants and band gaps.

	Lattice constant (Å)	Band gap (eV)
HfCoSb	6.0541	1.13
ZrCoSb	6.0945	1.06
HfIrSb	6.3288	0.89
ZrIrSb	6.3580	1.40

TABLE II: The calculated effective masses using the curvature of the band structure. The values related to the transport properties are given with the unit of m^*/m_e. Two values are calculated along different directions showing strong anisotropic bands.

type	**k**-point	band	HfCoSb	ZrCoSb	HfIrSb	ZrIrSb
p-type	Γ	VBM,VBM-1	3.4, 0.8		1.5, 0.6	1.7, 0.6
		VBM-2	0.2, 0.5		0.2, 0.3	0.2, 0.3
	L	VBM	5.0, 2.1	3.2, 2.1	7.3, 0.9	5.7, 1.1
		VBM-1	5.0, 0.9	3.2, 1.0	7.3, 0.4	5.7, 0.4
n-type	X	CBM	5.6, 0.9	5.4, 1.0	5.3, 1.8	1.1, 0.6
		CBM+1			0.8, 0.5	3.6, 2.2
	Γ	CBM			0.8,1.0	1.2, 1.0
	K	CBM				1.0